Magnetic Core Losses

The PSMA-Dartmouth Studies
Phase III Project

PSMA Magnetics Committee Core Loss Phase III Final Report

John H.Harris
Thayer School of Engineering
Dartmouth
20 March, 2013

Sponsored by
The Power Sources Manufacturers Association
email: power@psma.com
http://www.psma.com/
P.O. Box 418
Mendham, NJ 07945-0418
Tel: (973) 543-9660
Fax: (973) 543-6207

PSMA Magnetics Committee
Core Loss, Phase III
Final Report[1]

John H. Harris

20 March 2013

[1]Revision 310

Contents

List of Tables

List of Figures

1 Introduction

Phase III of PSMA Magnetics Committee Core Loss Project is a collection of small, exploratory subprojects. The project statement of work (SOW) lists five subprojects:

1. Test intentionally added parasitic impedances in the test equipment to see if they affect the data, with one representative core.
2. Test some winding variations in simulation and in practice, to see if they affect the data.
3. Additional testing with powder cores.
4. A series of tests with constant frequency and constant peak flux density (constant volt-seconds), but with varying on-time and voltage. These will be conducted for three cores.
5. Swap cores with ETH [Jonas Müehlethaler at ETH, Zürich], and try to duplicate each others' data.
6. Complete tests on the nanocrystaline core.

Of these, we were only able to conduct items 1, 2, and 5, with the available budget, primarily due to time spent on quality control tasks and consequential troubleshooting. These included testing experiment reproducibility, and measures to control possible sources of variation in the data. The conducted subprojects are discussed in the following sections

2 Parasitic Loss Experiment

From the project SOW:

1. Test intentionally added parasitic impedances in the test equipment to see if they affect the data, with one representative core.

The utility of this experiment is subtle—our basic approach to measuring core loss is immune to problems with the drive circuit because it measures the voltage due to flux (with the sense winding) and current *directly*, giving us a short inferential path to the instantaneous power and energy per cycle, but there are still some possible error sources:

1. We are trying to measure the core loss given a *particular* voltage waveform: a clean, square, pulse-width-modulated (PWM) waveform. Poor fidelity in applying that waveform could produce misleading results—the apparatus will faithfully report the core loss of whatever waveform is applied—even if it distorted.
2. There can be problems with the functioning and calibration of the test instruments.

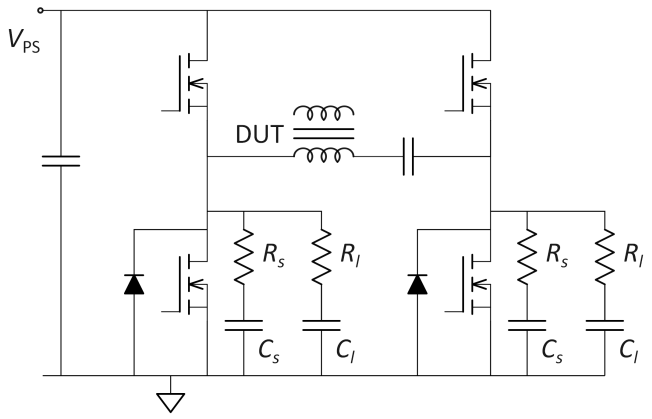

Figure 1: Drive bridge schematic detail showing the addition of "parasitic" loss capacitance, C_l, to the output terminals of the bridge. (Initially, $R_l = 0$.) The DUT is the wound core. Both output nodes are already fitted with snubbers, each comprising R_s and C_s.

3. The condition, maintenance, or configuration of the experimental equipment, or errors in procedure, could produce incidental errors in measurement.

This experiment detects effects any of these three categories. To conduct the experiment, we measured a wound device in the conventional way (the *baseline* run set) and then added bypass capacitance around the lower voltage legs of the drive bridge (Figure 1), and measured the same device again. Of course we would rather test this by *improving* the drive circuitry, rather than degrading it, but the present experiment can be implemented at a much lower cost. The idea is that if we marginally increase transient distortion and the results are substantially the same, then we have greater confidence in the original results.

2.1 Experimental Setup

Figure 1 shows a portion of the drive bridge, including the snubber network, $R_s = 3.6\,\Omega$ and $C_s = 1\,\text{nF}$, and the simulated "parasitic" loss capacitance, C_l. (The final experimental setup added a damping resistor, R_l. See Section 2.2.1). The drive transistors used in the bridge are International Rectifier IRF3706 MOSFETs, having a typical output capacitance $C_{\text{oss}} = 1.07\text{nF}$. It is paralleled with an On Semiconductor MBR1035 Schottky diode having a capacitance of about 250 pF at 12 V. Thus, each bridge output node has the combined parasitic capacitance of at least, $C_p = 2C_{\text{oss}} + C_d + C_s = 1.3\,\text{nF}$, bypassing the device under test (DUT). This added capacitance loses $2(C_p V_{\text{ps}}^2/2)$ at each transition, or $E_l = 2C_p V_{\text{ps}}^2$ per cycle.

To test the system with additional loss capacitance, we reran the same wound core used in run sets mi01-4, -5, and -6 (from the Phase II project). This core

Shape	Material	Mfg lot	A_e [mm^2]	height [mm]	d_o/d_i
40402TC	F	S00809	3.1	2.54	2.11
42206TC	F	PS0142	26.2	6.35	1.61
42206TC	P	S00841	26.2		
42206TC	R	n/a	26.2		

Table 1: Cores used in the experiments in Phase III were all manufactured by Magnetics, Inc., who provided the data above.

is of Magnetics Inc. R material, in the 42206-TC shape (Table 1), wound with 5 turns. In the present run sets, the bridge was switched at from 20 to 500 kHz. The power supply voltage ranged up to 12.5 V. At that voltage, with $C_l = 0$, E_l is about 0.5 μJ. Only the square waveforms were used.

The baseline run set (no added loss capacitors), was named mi01-7. To get a feeling for baseline parasitic capacitance loss, the highest measured core loss per cycle, E_{cyc} was 6.6 μJ; the baseline parasitic capacitance loss (due to C_p) is less than 8% (or 0.3 dB) of this core loss.

A second set, mi01-8, was identical, but with the added loss capacitors having $C_l = 1.0$ nF (but $R_l = 0$). The added loss capacitance, C_l, is on the order of C_p, but from a casual comparison of the conventional loss plots it appeared that the addition of C_l caused little change in the measured core losses.

To push it further, a third set was run, mi01-9, with $C_l = 4.7$ nF—over three times C_p, making the capacitive switching loss about 37% of the expected core loss. This gave us two incremental additions of loss that we could examine quantitatively. Around this point in the project, we began to notice problems with reproducibility, which are discussed in more detail in Section 2.2.

After modifying the apparatus for improved reproducibility, four baseline sets were run, mi01-7s, t, u, and v (Figure 2). Most of the baseline measurements were consistent within about ± 0.2 dB. With the parasitic loss setup, we obtained better waveform fidelity and reproducibility with the addition of $R_l = 3.3\,\Omega$. Three sets were run with this modification, mi01-11, -12, and -13. Figure 3 shows the deviation of the parasitic loss runs from the averages of the baseline runs. These sets tend to measure lower core loss, by about 0.2 dB, but the significance of this is difficult to assess with such a small sample. To keep this in perspective, the standard error for the two-plane Steinmetz curve fit for run mi01-7 was 0.4 dB (about $\pm 9.3\%$), while we have increased the capacitive switching loss by 1.4 dB (37%). We conclude that this experiment gives no evidence that variations in the drive bridge switching losses have a significant effect on our core loss measurements.

2.2 Reproducibility

This section is presented to aid in project management. The discussion is not quantitative, since the repair work was not the objective of the project, but

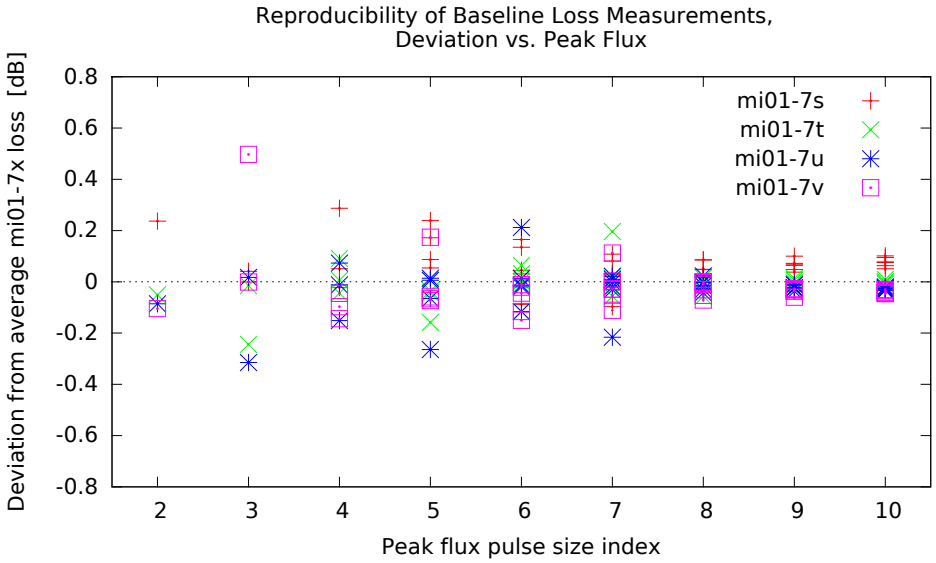

Figure 2: Deviation of baseline set losses from the average over the four runs sets.

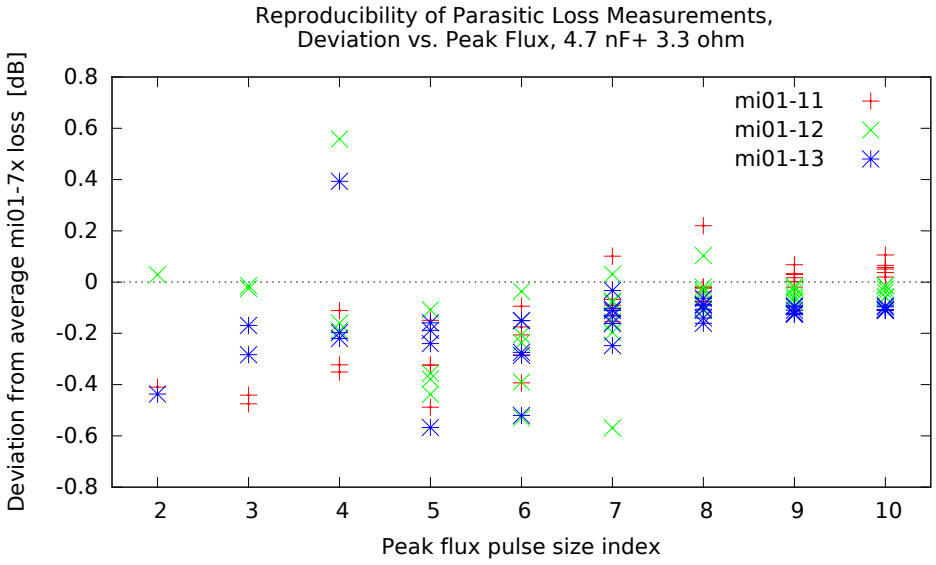

Figure 3: Deviation of parasitic loss runs with average losses of four baseline runs sets.

rather a hurdle that needed to be overcome to complete the investigation with confidence in the measurements.

Initial runs comparing measurements with and without added parasitics gave inconsistent results. Tracing the cause of these discrepancies accounts for most of the effort in the parasitic loss subproject. Three important effects where considered:

1. Chaotic waveform transients, caused by loss capacitance (C_l) ringing.
2. Marginal bridge MOSFET gate drive voltage.
3. Microphonic power-lead connector resistance.

Of these, the first and third had the greatest effect, but they are presented in the following sections in the order in which they were investigated.

2.2.1 Chaotic Waveform Transients

An initial test with $C_l = 1\,\text{nF}$ had a conventional core loss plot that looked qualitatively very similar to the baseline plot. To push it further, a third set was run, mi01-9, with $C_l = 4.7\,\text{nF}$—over three times C_p. This provided two incremental additions of loss that could be examined quantitatively. Plotting both the $C_l = 1\,\text{nF}$ and $4.7\,\text{nF}$ losses versus pulse width, showed a scattering of points, suggesting some kind of problem.

Looking for clues for this apparent anomaly, it is useful to examine the oscilloscope plots. Figures 4 and 5 show plots for runs mi01-7-001 and mi01-9-001, both for pulse width $t_1 = 1\,\mu\text{s}$ ($T = 2\,\mu\text{s}$). The most striking difference is the increased ringing, now at about 10 MHz.

If high-frequency ringing initiated by one switching transition is not sufficiently damped to be present at the next switching transition, the exact phasing between the ringing and the switching event can have a significant effect, and small jitter in timing can greatly change this phase if the ringing is at sufficiently high frequency.

To remedy this, a damping resistor was added, $R_l = 3.3\,\Omega$, which significantly improved reproducibility.

2.2.2 Marginal Gate Drive Voltage

Looking for reproducibility problems suggested problems with hardware reliability. There had been some problems with gate drive power supply battery contact resistance. The bridge circuit has four legs, two for connecting the DUT terminals to ground, and two for connecting device terminals to the power supply positive terminal, the *high side*. The ground-side gate drives have always been powered by the same 10 V power supply that runs the decoder logic and dead-time circuitry. The high-side gate drives "float"—they are referenced to the bridge output terminals, which range from 0 to 12.5 V above ground. In the original machine, (before August 2012) each high-side gate drive was powered by a single, rechargeable, 8.4 V Ni-MH battery.

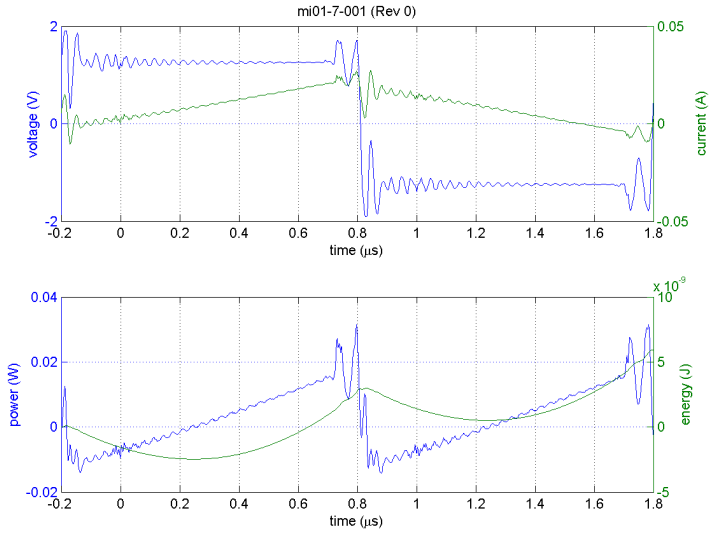

Figure 4: Routine test waveform (mi01-7-001) for 1 μs, and 1.25 V pulse.

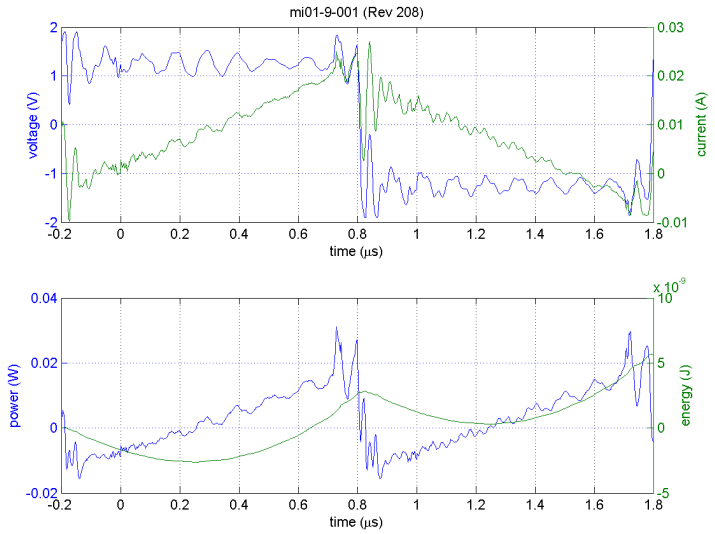

Figure 5: Lossy bridge waveform (mi01-9-001) for 1 μs, 1.25 V pulse, but with loss capacitance $C_l = 4.7$ nF.

That design could be vulnerable to battery charge-state variations, though it was not clear whether it was contributing to the observed reproducibility problems. To eliminate that possibility and to avoid the need to perform time-consuming testing to verify the extent of its importance, we added voltage regulators to the gate drive supplies.

To do this we added simple three-terminal regulators (Micrel Inc. MIC2940A), each referenced to its bridge output terminal. A second battery was added in series on each side, doubling the input voltage, to provide ample headroom for regulation, down to 12 V. After installing the new gate drive power supplies, the dead time timing was rechecked, and found to be satisfactory.

2.2.3 Power Supply Wiring

Some problems with reproducibility were traced to the wire leads between the programmable power supply and the bridge assembly. The wires were bolted to the power supply terminals, and fitted with banana plugs to connect to the bridge assembly. Both banana plugs were old, of low-quality manufacture, and had fatigued, flattened contact leaves. They fit so loosely in the jacks that it was impossible to measure a meaningful voltage drop across the connection. It may be that vibrations transmitted from the stirred oil coolant could have introduced microphonic noise into the applied drive voltage. These connectors were replaced with new, high-quality banana plugs, resulting in much improved reproducibility.

3 Winding Variations

From the project SOW:

2. Test some winding variations in simulation and in practice, to see if they affect the data.

We would like to see if a simpler flux geometry influences the "dead-time loss" phenomenon discovered in Phase I—losses for PWM waveforms having dead time (i.e., periods of zero drive voltage and constant flux) are greater than predicted by the composite waveform hypothesis. Most of the cores tested in this project in the past were toroidal, wound with about five turns in a simple, helical lay.

In this exploratory experiment we compare a typical five-turn toroidal-core device used in previous experiments, with an "equivalent," single-turn, "hairpin" device (Figure 6). The intent is to have a non-helical winding geometry, so that flux lines are oriented in the plane perpendicular to the wire. The hairpin core is not ideal (most notably, the geometry does not guarantee that the flux density is identical around the perimeter of the core, and it can be higher near return-path string of cores), but solves two problems:

1. With a single turn on our typical core geometry, the present apparatus can not supply enough current for our range of flux densities. To use the

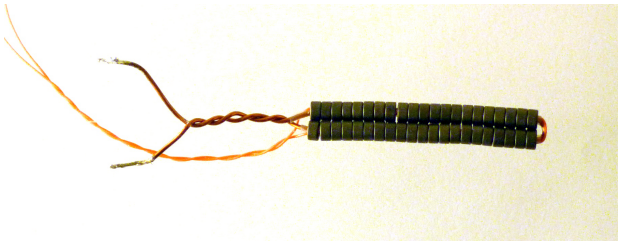

Figure 6: The hairpin test device. Forty-two bead cores were threaded on a hairpin-shaped piece of 18 AWG magnet wire.

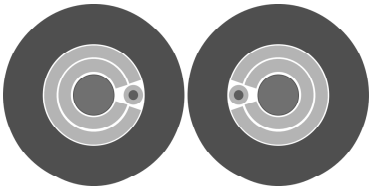

Figure 7: Cross-section of the hairpin test device.

existing equipment, we would like a core with about 1/5 the volume.

2. A pot-shaped winding is difficult to design and fabricate (more so at $\sqrt[3]{1/5}\times$ size).

3.1 The Hairpin Core

The hairpin device was fabricated by threading 21, 40402-shaped bead cores (Table 1) on each leg of a hairpin-shaped piece of 18 AWG magnet wire. To keep the drive wire centered in the core, two snug-fitting layers of PTFE tubing were added between the wire and beads. The sense winding was of stranded, 32 AWG, PTFE-insulated wire, parallel (but not concentric) to the drive wire (Figure 7). The total volume can be adjusted by varying the number of beads.

3.2 Hairpin Core Performance

The original run set from July 2010 was repeated in run set mi12-2, so the configuration of the apparatus would be up-to-date, and the same for all devices. In our first hairpin core run set (mi12-1), we used a 40-bead hairpin core (Figure 8, red +). There were large deviations from the toroidal core loss measurement. The scattered appearance of Figure 8, in which deviations are plotted against core loss, gives way to patterns when the deviation is plotted against peak flux (Figure 9).

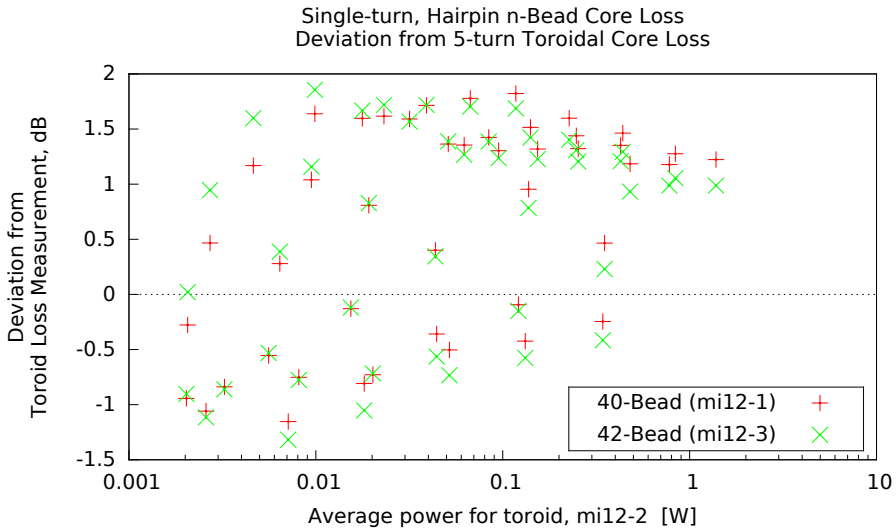

Figure 8: Hairpin core loss deviation vs. loss compared with a conventional, five-turn test device.

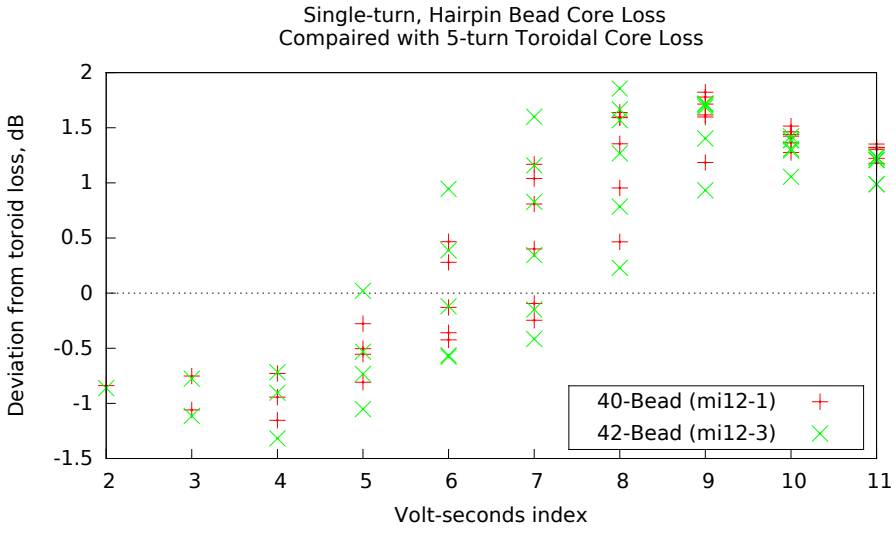

Figure 9: Hairpin core loss deviation vs. $\mathrm{V} \cdot \mathrm{s}$, compared with a conventional, five-turn test device. The volt-seconds index is a logarithmic measure of pulse width times amplitude.

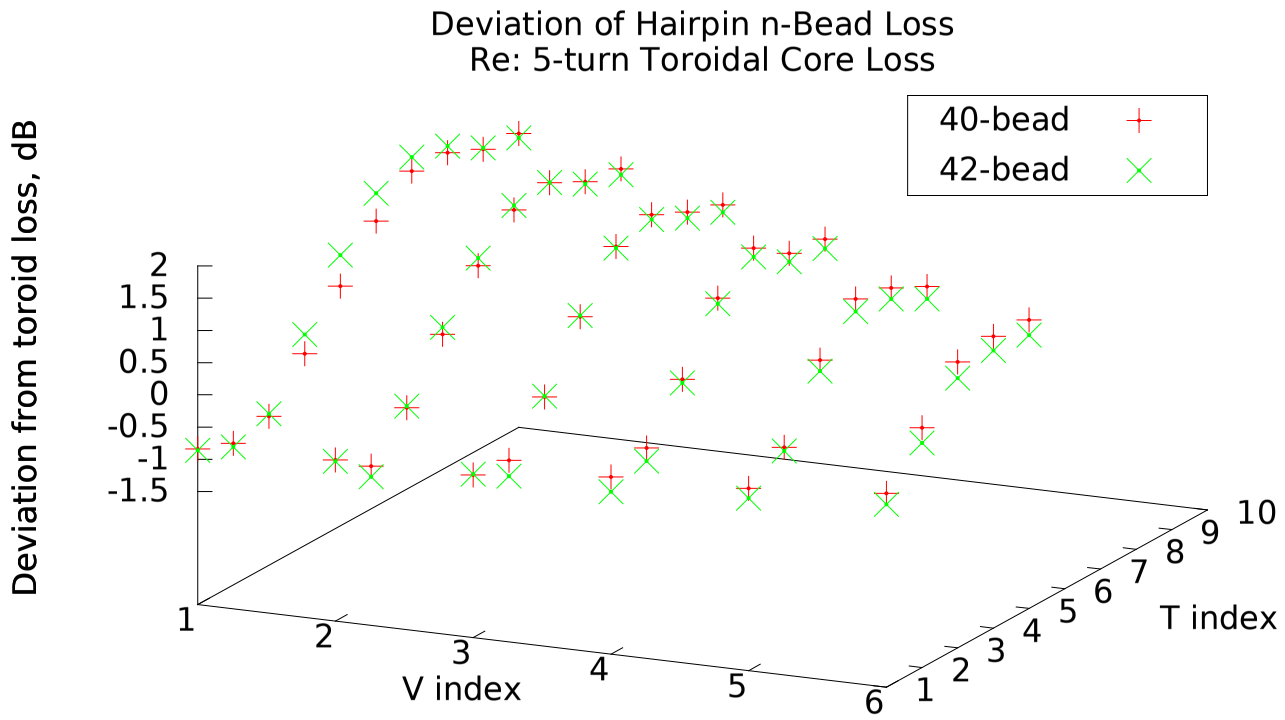

Figure 10: Hairpin core loss (3-D) compared with a conventional, five-turn test device. The V and T indices are logarithmic measures of pulse width and amplitude.

Comparing oscilloscope plots of for run 032 ($32\,\mu\mathrm{V}\cdot\mathrm{s}$ pulse) from both the hairpin and toroid core run sets (Figure 11) shows the sense voltages agree well, but the hairpin device has a lower inductance than the toroid; This would not account for the increased core loss, and suggests earlier saturation. This could be attributed to the different ratios of core inner to outer diameter, d_i/d_o, of the full-size and bead cores. The smaller d_i/d_o ratio of the bead core leads to greater flux crowding at the inside diameter, where saturation begins.

Comparing oscilloscope plots for run 027 confirms this (Figure 12). Run 027 drives the core harder, with an $80\,\mu\mathrm{V}\cdot\mathrm{s}$ pulse. Again the sense voltages agree well, but the hairpin core has a much higher peak current, and a more exaggerated rise in di/dt due to saturation.

Two more beads were added to create a 42-core device with larger total core cross-section area for run set mi12-3. Figure 9 shows these results with green xs. The results are similar to those with the 40-core device. Figure 10 separates drive pulse amplitude from width, adding another dimension. (The abscissa of Figure 9, "volt-seconds index" is just the sum of Figure 10's V and T indices.)

There are several effects that could account for the differences measured. More detailed modeling of these could help explain the differences.

- As noted above d_i/d_o is significantly lower for the hairpin cores, compared to the toroidal core (Table 1), which means a higher radial flux gradient for a given peak flux, resulting in an earlier onset of saturation. A one-dimensional (radial) analysis can account for this effect.

  An alternative approach to examining this effect would be to eliminate it by custom fabricating cores in two sizes, but with identical d_i/d_o, preferably from the same batch of material.

- With the onset of saturation, there is asymmetry in flux leakage, resulting in greater saturation in a localized region of the core where it is adjacent to the other core. A two-dimensional, finite-element analysis would be required to model this.

3.3 Effect on Dead-time Loss Behavior

While the hairpin device we fabricated is not an exact simulation of the 42206 core with a pot winding, it does capture the feature of interest—unlike a helically-wound toroidal device, the flux loops are predominately planar—and in *parallel* planes, at that (unlike the pot-shaped winding). The most direct indicator of the dead-time loss phenomenon is the expand waveform series of runs. Figures 13 and 14 show little qualitative difference between the toroidal and hairpin cores with this series. The hairpin core has somewhat less overall increase in loss (1.1 dB versus 2.0 dB for $32\mu\mathrm{V}\cdot\mathrm{s}$ pulses), but the overall shape of the curve is similar.

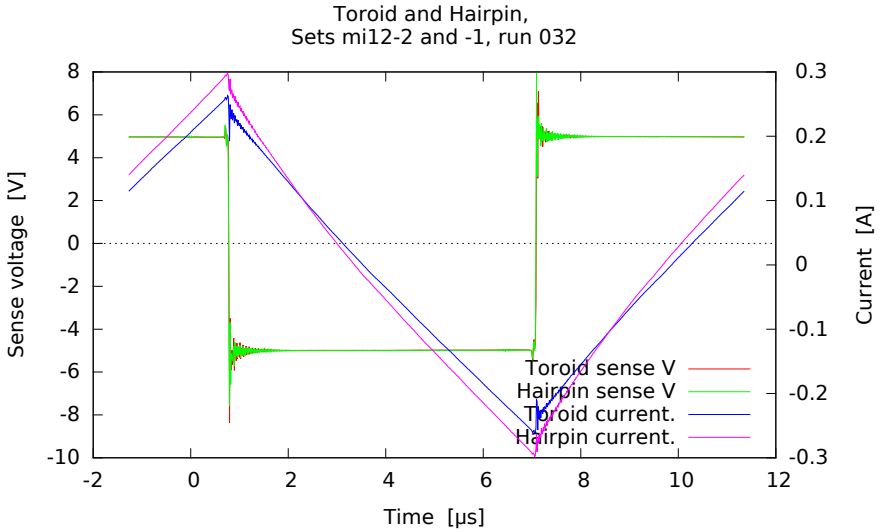

Figure 11: Comparison of hairpin and toroidal core oscilloscope plots for a $32\,\mu\mathrm{V}\cdot\mathrm{s}$ pulse.

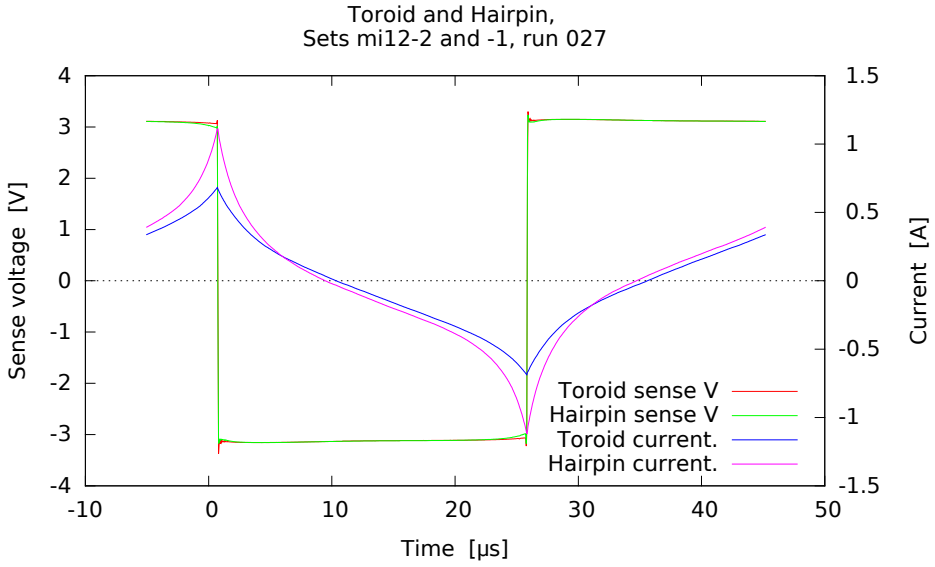

Figure 12: Comparison of hairpin and toroidal core oscilloscope plots for an $80\,\mu\mathrm{V}\cdot\mathrm{s}$ pulse.

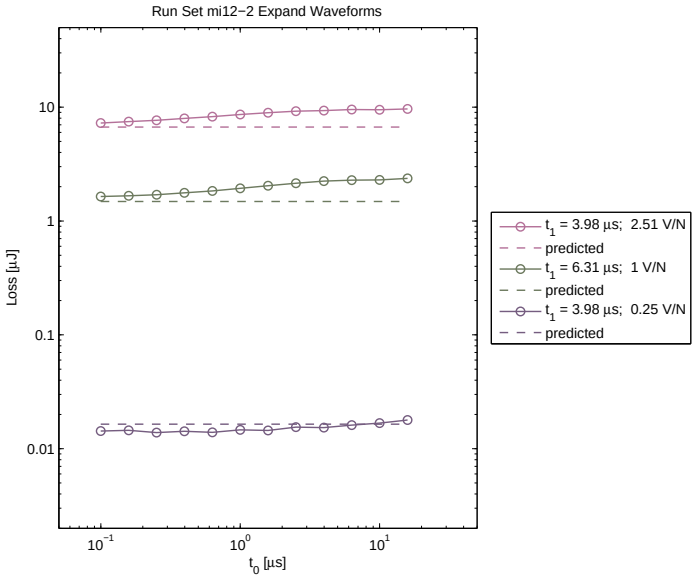

Figure 13: Expand waveform losses with the toroidal core. The plot shows core losses for PWM waveforms having identical peak flux, but differing dead times.

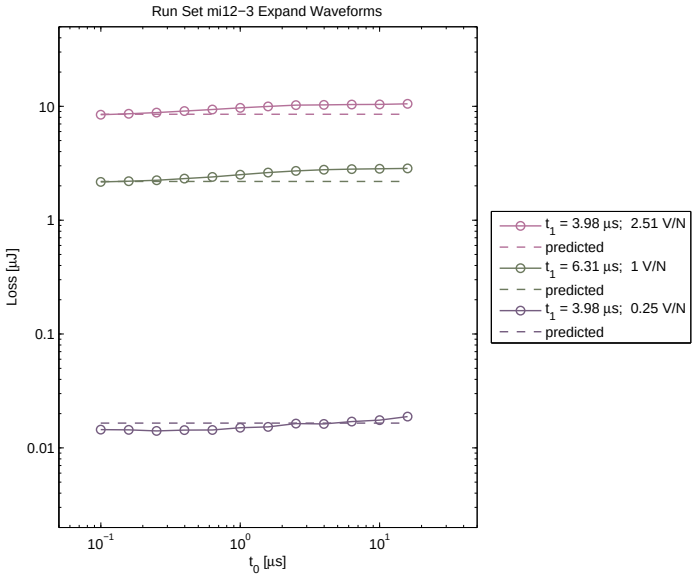

Figure 14: Expand waveform losses with the hairpin core.

4 Independent Testing

To get an independent check on the reproducibility of our results, we wound two devices to be measured first with our apparatus, and then shipped to Jonas Müehlethaler at ETH, Zürich, for testing on their apparatus. Both cores were wound with 5 turns, on cores manufactured by Magnetics, Inc., in their 42206 toroidal shape, one each from the F and P materials (Table 1, run sets mi05-6 and mi03-2, respectively).

5 Data Availability

The data have been supplied if the same format as was used in Phase II, and will be available at `http://engineering.dartmouth.edu/inductor/psma/`. Table 2 summarizes the run sets added in Phase III. Data gathered using the unimproved drive electronics was used only for diagnosis, and will not be posted.

Subproject Set IDs	Description
Parasitic loss comparison.	
mi01-7	Original baseline run set to be compared with loss capacitor sets. This run set was not posted, having been replaced by set mi01-7v.
mi01-7x	Series of baseline run sets, $x = \{$s, t, u, v$\}$, using the improved bridge electronics, to check for reproducibility.
mi01-8	The initial lossy-bridge run set, with $C_l = 1\,\mathrm{nF}$, $R_l = 0$. Not posted.
mi01-9, -10	$C_l = 4.7\,\mathrm{nF}$, $R_l = 0$. Not posted.
mi01-11, -12, -13	Series of lossy-bridge run sets with $C_l = 4.7\,\mathrm{nF}$, $R_l = 3.3\Omega$.
Hairpin core.	
mi12-1	Forty-bead hairpin core.
mi12-2	Baseline 5-turn toroidal core.
mi12-3	Forty-two-bead hairpin core.
Independent testing.	
mi03-2	0P42206 core with 5 turns.
mi05-6	0F42206 core with 5 turns.

Table 2: Runs sets added in Phase III. Runs sets with the unimproved drive electronics have not been posed on the data web page.